IEEE Access
Multidisciplinary | Rapid Review | Open Access Journal

Received 1 November 2023, accepted 4 December 2023, date of publication 12 December 2023,
date of current version 27 December 2023.

Digital Object Identifier 10.1109/ACCESS.2023.3341509

RESEARCH ARTICLE

Development and Optimization of a Two-Degree-of-Freedom Piezoelectric Harvester Based on Parallel Cantilever Structure With Magnetic Coupling

YILI HU[1], YARU DING[1], NAN WEI[1], XINHUI LI[2], JIANPING LI[1], (Member, IEEE), JIJIE MA[1], ZHONGHUA ZHANG[1], GUANGMING CHENG[1], AND JIANMING WEN[1]

[1]Institute of Precision Machinery and Smart Structure, Key Laboratory of Intelligent Operation and Maintenance Technology and Equipment for Urban Rail Transit of Zhejiang Province, College of Engineering, Zhejiang Normal University, Jinhua 321004, China
[2]Xingzhi College Zhejiang Normal University, China Electrical Engineering Department, University of Colorado at Boulder, Boulder, CO 80309, USA

Corresponding author: Jianming Wen (wjming@zjnu.cn)

This work was supported in part by the Zhejiang Provincial Natural Science Foundation of China under Grant LQ21E050013 and Grant LY20E050009, in part by the Zhejiang Provincial Key Research and Development Project of China under Grant 2021C01187, in part by the National Natural Science Foundation of China under Grant 52205075, and in part by the National College Students' Innovation and Entrepreneurship Training Program under Grant 202310345039.

ABSTRACT Vibration energy harvesting using the piezoelectric effect has recently attracted significant attention from scholars. The main concern in the research of piezoelectric vibration energy harvesters is to improve the operating bandwidth and output power in low-frequency vibration environments with random and time-varying nature. A novel piezoelectric vibration energy harvester (PVEH) with three parallel cantilevers and repulsive magnet pair structures is proposed in this work to achieve the above goal. The proposed PVEH has the potential to take full advantage of the synergistic effect of the multi-frequency and magnetic nonlinear performance enhancement techniques. The characteristics of the harvester are systematically studied by theoretical modeling, simulation, and experiments. The influence of the critical parameters (i.e. the tip mass of the inner beam, the tip mass of the outer beam, and the magnet spacing) on the output performance of the PVEH is discussed and optimized in detail, and then the internal mechanism of the proposed energy harvesting method based on multi-frequency and magnetic cooperation is revealed. The results show that the improvement rate of the output power of the fabricated prototype under the condition of first-order and second-order operating frequency reaches 23.35% and 38.10%, respectively, compared with the non-magnetic structure. Finally, the optimal configuration of the harvester ($M_i = 6.70$ g, $M_o = 5.00$ g, $s = 22$ mm) obtains a maximum half-power bandwidth of 1.052 Hz and a maximum output power of 2.80 mW under 0.2g with 0.155 MΩ load resistance. The proposed energy harvesting system is expected to be a promising alternative to efficient vibration energy harvesters.

INDEX TERMS Piezoelectric, energy harvester, parallel, multimodal, magnetic coupling.

I. INTRODUCTION

For the past few years, the proliferation of mobile electronic devices, sensor networks, and the Internet of Things (IoT) has generated the blossom of the self-powered energy harvester. The energy sources of the self-powered energy harvester are recyclable and renewable, which is different from the environmental pollution resulting from fossil fuel consumption and the limited lifespan of batteries. Vibration energy, as a typical representative energy source of a self-powered energy harvester, has the characteristics of environmental protection, widespread existence, and weather resistance. So,

The associate editor coordinating the review of this manuscript and approving it for publication was Michail Kiziroglou.

it has become one of the current research emphases of energy harvester. Based on different working principles, vibration energy harvesters are usually divided into electromagnetic [1], electrostatic [2], triboelectric [3], magnetostrictive [4], and piezoelectric [5] forms. In these categories, piezoelectric vibration energy harvester (PVEH) has attracted keen attention because of its significant advantages, such as high energy density, strong electromechanical coupling, simple structure, and easy integration [6], [7], [8]. Traditional PVEHs are typically designed as single-degree-of-freedom linear structures such as cantilever beams. Among many application scenarios, ambient vibration frequencies are low-frequency and narrow bandwidth mostly. Therefore, a desired PVEH should own a broadband working frequency and large output under weak excitation. One of the effective ways to improve the output performance of PVEH is to match its operating frequency with the ambient frequency range. However, this general linear piezoelectric energy harvesting system is commonly limited to a narrow frequency bandwidth [9], [10], [11]. When facing the above dilemma, various performance enhancement techniques have been proposed and studied to help traditional PVEH achieve broadband bandwidth and improve energy harvesting efficiency, mainly including multimodal [12], [13], frequency tuning [14], [15], [16], frequency up conversion [17], [18], [19], [20] and nonlinear techniques [21], [22], [23], [24], [25].

The multimodal technique has been a universal strategy for piezoelectric energy harvesters to enhance output power and expand bandwidth by designing various structures. The main mechanisms are a multi-frequency energy harvester through the aggregation of multiple beams [26], [27] and a multidirectional energy harvester [28]. Toyabur et al. [29] described a multimodal piezoelectric energy harvester with four secondary beams attached to one primary beam with a low excitation frequency range. Raja et al. [30] designed a multimodal PVEH consisting of a reversed exponentially tapered beam (primary beam) and six branched beams (secondary beams) attached to the free end of the primary beam with a proper flange. The multimodal PVEH provided broadband with densely placed vibration modes while the output voltages varied from 24.5 V to 2.69 V at mode frequencies in the 8-30 Hz range. Huang et al. [31] proposed a multi-mode broadband piezoelectric vibration energy harvester composed of five tip masses, two U-shaped cantilever beams, and a straight beam. This study showed that tip masses and the length of the cantilever beam had an essential impact on widening the bandwidth. From the experimental results, the harvester had five resonant frequencies of 13, 15, 18, 21, and 24 Hz, which corresponded to the maximum output power of 52.2, 49.4, 61.3, 39.2, and 32.1 μW severally under the acceleration of 0.5g. Besides, some PVEHs had been devised to obtain multidirectional energy. For example, Zhou et al. [32] presented a flexible longitudinal zigzag PVEH for obtaining multidirectional vibration energy. Among the works mentioned above, although significant progress has been made towards expanding the bandwidth of PVEH, there still exists some common problems for the multi-frequency energy harvester: the effective bandwidth of each peak near the natural frequency remains relatively low. Besides, the output power of these kinds of devices could still be enhanced further. The main reason for these devices is that only a main cantilever beam plays a significant role in the output power [30].

On the other hand, the nonlinear technique has also aroused the interest of abundant scholars in piezoelectric energy harvesting because of its high gain ability to output performance. Magnetic structures can achieve nonlinear states such as monostable, bi-stable, and multi-stable in one system [33], [34], [35]. Lan et al. [33] investigated a monostable piezoelectric energy harvester consisting of a cantilever beam with a magnet on the free end and another repulsive magnet fixed on the base. This scheme had a power performance enhancement and bandwidth enlargement. Wang and Tang [34] proposed a four-magnet bi-stable piezoelectric energy harvester consisting of a piezoelectric cantilever beam with a tip magnet, a fixed magnet, and two movable magnets. The results showed that FBEH can enhance harvesting performance in low excitations by selecting suitable parameters. Zhu et al. [35] proposed a hybrid tri-stable piezoelectric vibration energy harvester (T-PVEH). The T-PVEH had a cantilevered beam, a tip magnet, and two external magnets. The study concluded that an appropriate range of the magnetic distance could improve the effective bandwidth and harvested power of the global inter-well motions while the stable global inter-well motions completely disappear beyond this range. The above studies have indicated that the nonlinear technique could broaden the effective bandwidth of each peak near the natural frequency. However, the apparent problem is that the output power of each peak near the natural frequency has been decreased, which is the result of reducing the power peaks to broaden the bandwidth for each peak near the natural frequency [36].

Previous studies have shown that both the multimodal and nonlinear techniques have merit and demerit. The multi-frequency technique has a narrow bandwidth and high output power for peaks near the natural frequency. In contrast, the nonlinear technique has a wide bandwidth and output power for peaks near the natural frequency, which inspires some scholars to utilize the characteristics of the multi-frequency technique and nonlinear technique to complement each other Lim and Yoo [37] had invented a M-shaped PVEH with two sets of magnets. The PVEH had a single prominent peak or broadband frequency response characteristic by controlling the magnet spacing. The experimental results indicated that the proposed PVEH achieved much higher power generation performance around the natural frequency range of 15-22 Hz than the cantilever harvester. Fan et al. [38] utilized two magnetically coupled piezoelectric cantilever beams with orthogonal deflection directions to create a compact bi-directional nonlinear PEH sensitive

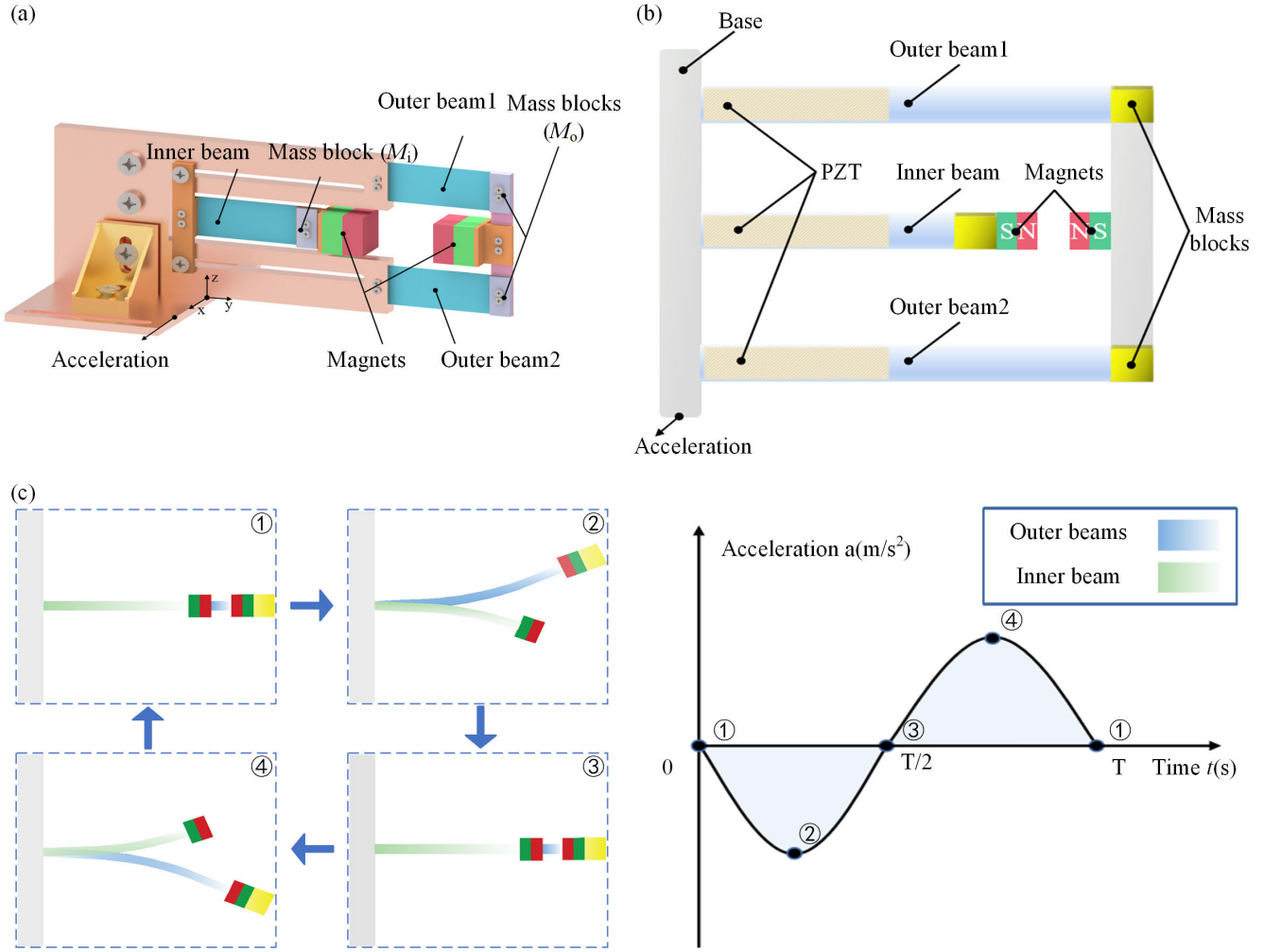

FIGURE 1. Structure and principle of the proposed PVEH: (a)The 3D diagram of the model; (b) The main view of the structure; (c) Working principle.

to two orthogonal directions. The proposed PVEH could not only harvest energy from various directional vibrations but also improve the output performance of the voltage as compared to its linear counterpart. However, their effective bandwidth was concentrated in a relatively high-frequency band, about 35-40 Hz, and the output voltage below 25 Hz was close to none. He and Jiang [39] proposed a complementary multi-mode low-frequency PVEH, mainly composed of three chiral folded beams in a light hexagonal matrix. The designed PVEH could acquire four resonant peaks in the frequency response by importing external magnetic force. At the same time, response peaks could move toward the low frequency and change in values. However, this work needs an in-depth study of the coupling relationship between magnetic force and mechanical vibration. From the above studies, combining multimodal and nonlinear techniques has the apparent advantage of more comprehensive broadband and better output performance than the single technique. Nonetheless, it is necessary to systematically explain the natural mechanisms regarding the synergy of the multimodal and nonlinear techniques that can achieve broadband and determine the relevant parameters and laws that affect the output power of PVEH.

A two-degree-of-freedom piezoelectric harvester based on a parallel cantilever structure with magnetic coupling is designed and developed to achieve the above targets. In terms of the former studies, it has been initially determined that the tip mass of the beams and the magnet spacing are the key parameters affecting the output power of the PVEH. This article systematically explores the influence of these parameters on the coupling mechanism and finds better methods to optimize output power and broaden the frequency band. The rest of this article is organized below. The second section recommends the model structure and working principle of the proposed PVEH. In the third section, the theoretical energy harvester model is established to make numerical simulation analysis and probe the influence regularity of critical parameters on output performance. The fourth section constructs an experimental system to determine the accuracy of theoretical analysis results and systematically optimize the

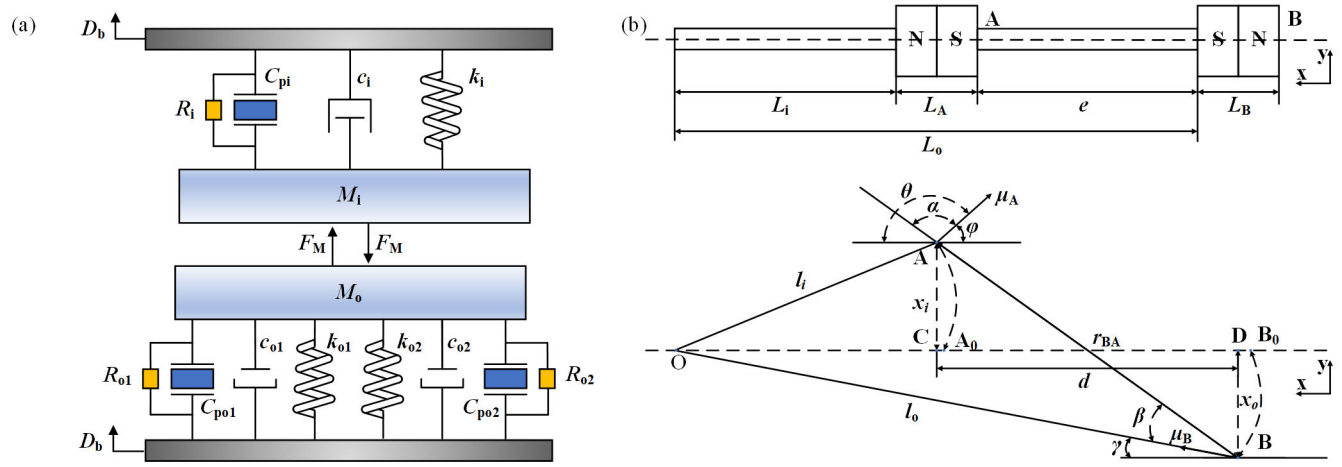

FIGURE 2. (a) Equivalent model of the proposed PVEH;(b) The top view of the structure diagram and the analysis of the simplified model for the magnet pair.

output performance of the proposed PVEH. The last section concludes the work of the study.

II. STRUCTURE AND MODELING OF THE PROPOSED PVEH

The presented parallel PVEH is based on multi-frequency and magnetic nonlinear techniques, which consists of two parts: three cantilever beams with the tip masses and a pair of repulsive magnets, as sketched in Fig. 1(a) and Fig. 1(b). Three cantilever beams can be divided into the inner beam and the outer beams, which means the PVEH integrates at least two frequencies. With the change of the mass block loaded on the free end of the beams, the effect of tip mass on the output performance of the PVEH can be explored. A pair of repulsive magnets are placed at the free end of the inner and outer beams, respectively, to enhance the amplitudes, and a suitable magnet spacing can be selected by adjusting the position of the inner beam.

A schematic diagram (Fig. 1(c)) illustrates the working principle of the parallel PVEH. Under the excitation of the sinusoidal signal, this PVEH has four states of motion in one cycle, as shown below.

Step 1: When $t = 0$ s at point one, the PVEH is in state ①, which means the inner and outer beams are in the central equilibrium position. From $t = 0$ s to $t =$ T/4 s, a downward and increasing excitation acceleration acts on the harvester. At this time, the outer beams deform and bend upward because the tip mass blocks on the outer beams are heavier than the inner beams. In contrast, the inner beams bend downward due to the repulsive magnetic force exerted.

Step 2: When $t =$ T/4 s at point two, the PVEH lies in state ②. At this moment, a downward bending deformation of the inner beam reaches the lowest limit position. Meanwhile, the outer beams with an upward bending deformation reach the highest limit position. From the $t =$ T/4 s to $t =$ T/2 s, a downward and decreasing excitation acceleration plays a role in the harvester. By this time, the inner beam moves upwards and tends to the central equilibrium position. At the same time, the outer beams move downward and tend to the central equilibrium position either.

Step 3: When $t =$ T/2 s at point three, the PVEH is at state ③. The motor process of this stage is an inverse process of Step 1.

Step 4: When $t = 3$ T/4 s at point four, the PVEH is located in state ④. The movement of this stage rolls back the process of Step 2. Finally, it returns to the state at point one.

So far, above is the working condition of the energy harvester in a single working cycle. The presented PVEH will repeat the operation depending on this work cycle.

The equivalent model of the harvester and magnetic simplified model has been established as shown in Fig. 2 from the structure of this parallel PVEH, where the subscripts about o1, o2, i express the first outer beam, second outer beam, and inner beam severally. Based on the equivalent model, the mechanical and electrical governing equations of the parallel PVEH are written as follows, where D_o and D_i are the tip displacement of the cantilever beams. U_{o1}, $U_{o2,}$ and U_i are the output voltage across the external resistive load R_{o1}, $R_{o2,}$ and R_i. In addition, some equivalent parameters of the system are included in governing equations (1). The equivalent tip masses of the

$$\begin{cases} M_o\ddot{D}_o = -k_{o1}\left(D_o - D_b\right) - k_{o2}\left(D_o - D_b\right) - c_{o1}\left(\dot{D}_o - \dot{D}_b\right) \\ \quad -c_{o2}\left(\dot{D}_o - \dot{D}_b\right) - \alpha U_{o1} - \alpha U_{o2} - F_M \\ M_i\ddot{D}_i = -k_i\left(D_i - D_b\right) - c_i\left(\dot{D}_i - \dot{D}_b\right) - \alpha U_i + F_M \\ U_{o1}/R_{o1} = \alpha\left(\dot{D}_o - \dot{D}_b\right) - C_{po1}\dot{U}_{o1} \\ U_{o2}/R_{o2} = \alpha\left(\dot{D}_o - \dot{D}_b\right) - C_{po2}\dot{U}_{o2} \\ U_i/R_i = \alpha\left(\dot{D}_i - \dot{D}_b\right) - C_{pi}\dot{U}_i \end{cases} \tag{1}$$

cantilever beams are M_o and M_i. k_{o1}, $k_{o2,}$ and k_i express the equivalent stiffness. c_{o1}, $c_{o2,}$ and c_i are represented as the damping of the beam and α means the electromechanical coupling coefficient. C_{po1}, $C_{po2,}$ and C_{pi} refer to the capacitance

of the piezoelectric beams. Besides, D_b and F_M denote the displacement of the base and the repulsive force between the two magnets.

Apart from the magnetic force, some related references [40], [41] indicate that the vast majority of the equivalent parameters can be computed from the following equations combined with the basic structural and material parameters of the cantilever beam ($k_{eq} = 3EI/L^3$, $m_{eq} = 33/140mL+M_t$, $c_{eq} = 2\zeta\sqrt{k\text{eq}/m_{eq}}m_{ep}$, $\alpha = 2e_{31}bh_{pcb}$, $C_p = 2\varepsilon^s_{33}bL/h_p$), of which M_t, ε^s_{33}, b, e_{31}, h_{pcb} and h_p successively signify the tip mass, the clamped dielectric constant, the width of the beam, the piezoelectric constant in stress form, the distance from the center of the piezoelectric layer to the central axis of the beam, the thickness of piezoelectric layer.

Some magnetic force relationships must be established for derivation to obtain the magnetic force. Reference [42] shows that magnetism is related to the spacing between two magnets. Especially, there is a direct, intimate correlation between the spacing (s) and the displacement of the inner beam. From the simplified model that consists of three cantilever beams with a pair of magnets fixed on their free end, as shown in Fig. 2(b), some relevant formulas about magnetic force can be built. The magnetic flux density generated by magnet B on magnet A is expressed as (2), and the magnetic interaction potential energy is acquired as (3) [43], where $\boldsymbol{\mu}_0$ is the vacuumed permeability, $\boldsymbol{\mu}_A$ and $\boldsymbol{\mu}_B$ are the magnetic moment vectors, and $\boldsymbol{r}_{BA}$ is the distance from the source of $\boldsymbol{\mu}_B$ to $\boldsymbol{\mu}_A$.

$$\boldsymbol{B}_{BA} = -\frac{\mu_0}{4\pi}\nabla\frac{\boldsymbol{\mu}_B \cdot \boldsymbol{r}_{BA}}{r^3_{BA}} \tag{2}$$

$$U_m = -\boldsymbol{B}_{BA} \cdot \boldsymbol{\mu}_A \tag{3}$$

The magnetic force that dipole B produces on dipole A is obtained from potential energy as follows (4) [44]. Substituting (2) and (3) into (4), thus the force expression can be derived as (5).

$$\boldsymbol{F} = -\nabla U_m \tag{4}$$

$$\boldsymbol{F} = -\frac{\mu_0}{4\pi}\nabla\left[\nabla\left(\frac{\boldsymbol{\mu}_B \cdot \boldsymbol{r}_{BA}}{r^3_{BA}}\right)\cdot\boldsymbol{\mu}_A\right] \tag{5}$$

From the reference [42], (5) can be simplified to (6), where $\hat{\boldsymbol{r}}_{BA}$ represents the unit vectors in the orientation of $\boldsymbol{r}_{BA}$. The correlative angles in Fig. 2(b) can replace each vector in (6), and (7) can be obtained through conversions. The vertical component of magnetic force in the y direction is expressed as (8), equal to F_M.

$$\boldsymbol{F} = \frac{3\mu_0\mu_A\mu_B}{4\pi r^4_{BA}}\left[\hat{\boldsymbol{r}}_{BA}\left(\boldsymbol{\mu}_B\cdot\boldsymbol{\mu}_A\right) + \boldsymbol{\mu}_B\left(\boldsymbol{\mu}_A\cdot\hat{\boldsymbol{r}}_{BA}\right) + \boldsymbol{\mu}_A\left(\boldsymbol{\mu}_B\cdot\hat{\boldsymbol{r}}_{BA}\right) - 5\hat{\boldsymbol{r}}_{BA}\left(\boldsymbol{\mu}_A\cdot\hat{\boldsymbol{r}}_{BA}\right)\left(\boldsymbol{\mu}_B\cdot\hat{\boldsymbol{r}}_{BA}\right)\right] \tag{6}$$

$$\boldsymbol{F} = \frac{3\mu_0\mu_A\mu_B}{4\pi r^4_{BA}}\left[\hat{\boldsymbol{r}}_{BA}\cos(\beta+\alpha) + \boldsymbol{\mu}_B\cos\alpha + \boldsymbol{\mu}_A\cos\beta - 5\hat{\boldsymbol{r}}_{BA}\cos\alpha\cos\beta\right] \tag{7}$$

$$F_y = \frac{3\mu_0\mu_A\mu_B}{4\pi r^4_{BA}}\left[(\cos(\beta+\alpha) - 5\cos\alpha\cos\beta)\sin(\theta-\alpha) + \cos\alpha\sin\gamma + \cos\beta\sin\varphi\right] \tag{8}$$

The (9) to (12) can be established based on the simplified structure model in Fig. 2(b).

$$l_i = \mathrm{OA} = L_i + \frac{L_A}{2} \tag{9}$$

$$l_o = \mathrm{OB} = L_o + \frac{L_B}{2} \tag{10}$$

$$d = \mathrm{CD} = \mathrm{CB}_0 - \mathrm{DB}_0 = e + \frac{L_A}{2} + \frac{L_B}{2} + L_i\cdot(1-\cos\varphi) - L_o\cdot(1-\cos\gamma) \tag{11}$$

$$r_{BA} = \mathrm{BA} = \sqrt{(x_i+x_o)^2 + d^2} \tag{12}$$

According to the trigonometric relations, (9)–(12) [42] can be substituted into (8), where x_i and x_o represent the distance of the AC and BD separately. Therefore, the expression of F_M can be given as (13) [42].

Substituting the expression of F_M into (1), then (1) will become a system of equations with five unknown variables and five equations, which means Equation 1 can be solved. After that, the numerical solution could be gained by employing the software Maple to calculate these governing equations.

$$F_M = \frac{3\mu_0\mu_A\mu_B}{4\pi r^5_{BA} l_i l_o}\left[2x_ix_o(x_i+x_o) + x_id\sqrt{l_o^2-x_o^2} - x_od\sqrt{l_i^2-x_i^2} + \frac{x_i+x_o}{r^2_{BA}}\left(x_ix_o\left(d^2-4(x_i+x_o)^2\right) + \sqrt{l_o^2-x_o^2}\sqrt{l_i^2-x_i^2}\left(4d^2-(x_i+x_o)^2\right) + 5d(x_i+x_o)\left(x_o\sqrt{l_i^2-x_i^2} - x_i\sqrt{l_o^2-x_o^2}\right)\right)\right] \tag{13}$$

III. SIMULATION OF THE PROPOSED PVEH

According to the theoretical analysis, (1) and (13) respectively show that tip masses and magnet spacing are the critical factors affecting the multi-frequency and magnetic nonlinear characterizations of the PVEH. This section mainly explored the influence law of the tip masses and magnet spacing on the open-circuit output voltages. In this simulation, the output voltages are the peak-to-peak values. Fig. 3 shows the simulation results of the open-circuit output voltages about the different tip masses of the beams under the ideal conditions of ignoring the voltage loss caused by the phase difference, where M_i and M_o express the tip mass of the inner beam and outer beams severally, U_i and U_o are the voltage of the inner beam and outer beam respectively and U represents the sum of the voltage of the inner beam and outer beams.

The frequency scans from 5 Hz to 15 Hz under the excitation of 0.2 g. Fig. 3a1 shows that the natural frequency of the inner beam has declined from 14.2 Hz to 9 Hz under changing the M_i from 2.5 g to 6.7 g. Both the first and second open-circuit output voltage peaks grow. As shown in Fig. 3a2, the natural frequency of the outer beam has little change while the first open-circuit output voltage peak gradually decreases and the second open-circuit output voltage peak increases.

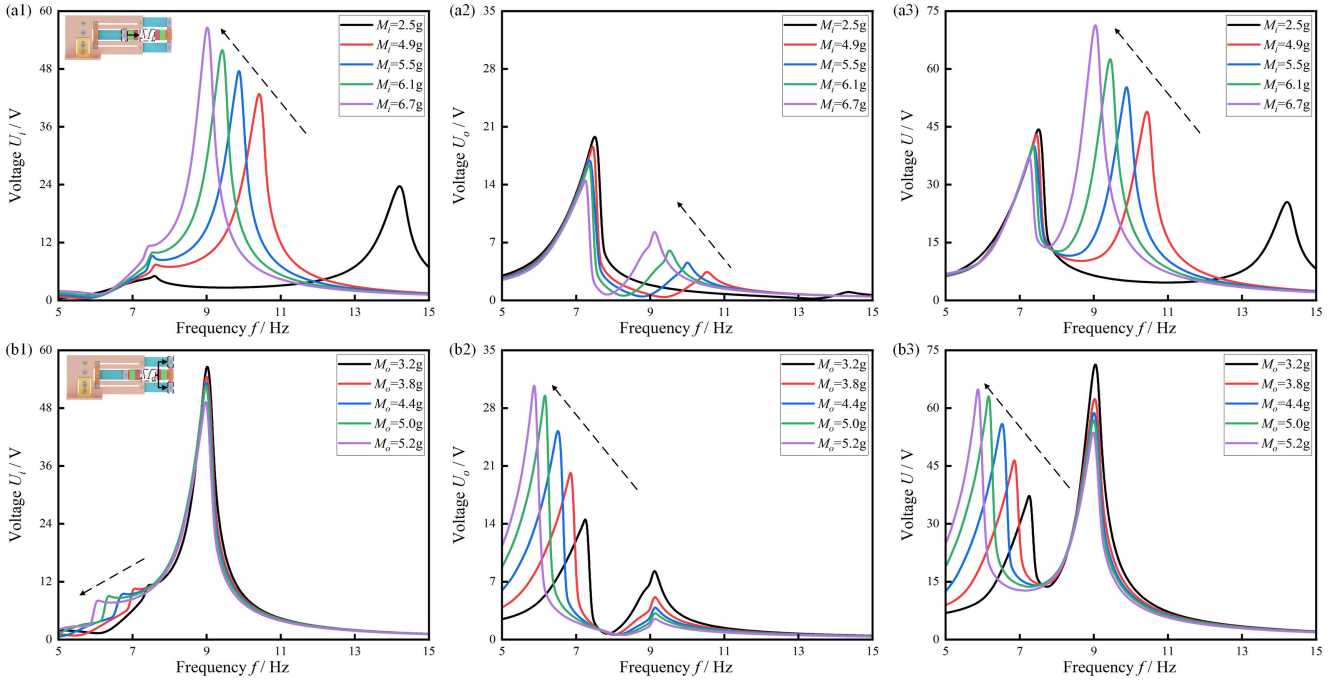

FIGURE 3. The simulation open-circuit output voltage under changing the tip mass of beams where s = 25 mm: (a1) The output voltage of the inner beam under changing the tip mass of the inner beam; (a2) The output voltage of the outer beam under changing the tip mass of the inner beam; (a3) The total output voltage of the inner beam and outer beams under changing the tip mass of the inner beam; (b1) The output voltage of the inner beam under changing the tip mass of the outer beam; (b2) The output voltage of the outer beam under changing the tip mass of the outer beam; (b3) The total output voltage of the inner beam and outer beams under changing the tip mass of the outer beam.

Generally, the increase of the tip mass of the inner beam can improve its output voltage and reduce the natural frequency. The output voltage under the $M_{\mathrm{i}} = 6.7$ g is better than the output voltage under the other tip mass of the inner beam in Fig. 3(a3). Thus, $M_{\mathrm{i}} = 6.7$ g has been a quality condition in the simulation experiment of exploring the effect of M_{o} on the output performance of PVEH.

As shown in Fig. 3(b2), the natural frequency of the outer beam decreases from 7.4 Hz to 6 Hz when M_{o} increases from 3.2 g to 5.2 g. The first open-circuit output voltage peak caused by the outer beams increases significantly, and the second open-circuit output voltage peak decreases. However, the first and second open-circuit output voltage peaks caused by the inner beam reduce slowly, as shown in Fig. 3(b1). Therefore, with the tip masses of the outer beam increase, the open-circuit output voltage produced by the outer beam at its natural frequency will be added. But it has little inhibitory effects on the inner beam. Fig. 3(b3) compares the output voltage under $M_{\mathrm{o}} = 5.0$ g and $M_{\mathrm{o}} = 5.2$ g, the output voltage of the entire system is similar. Considering the portability of the system, $M_{\mathrm{o}} = 5.0$ g is selected and has been an initial condition on the simulation experiment of Fig. 4. Fig. 3(a1)-(b3) expresses that both the open-circuit output voltage of the inner beam and outer beams have two peaks. The first voltage peak in Fig. 3(a1) and Fig. 3(b1) is created by the vibration of the inner beam, which is produced by the resonant of the outer beam under the effect of magnetic coupling. While the second peak in Fig. 3(a1), (b1) is made by the resonant of the inner beam. On the contrary, the resonant of the outer beam produces the first peak in Fig. 3(a2) and Fig. 3(b2). The resonance of the outer beam strengthens the vibration of the inner beam with the effect of magnetic coupling, which creates the second voltage peak. It can be found that both the natural frequency of the inner beam and the outer beam are included in the sweep frequency (5 Hz-15 Hz).

When the magnet spacing between the magnets gradually decreases from 35 mm to 22 mm, the first and the second open-circuit output voltage peak of the inner beam increases rapidly in Fig. 4(a). The spacing between the outer and the inner beam is 22 mm when no magnet is used. Fig. 4(b) shows that the first voltage peak of the outer beams decreases slowly, and the second voltage peak grows steadily. In Fig. 4(c), as the magnet spacing gradually decreases to a suitable range from $s = 25$ mm to $s = 22$ mm, the second voltage peak increases significantly because the magnetic force strongly affects the inner beam. In contrast, the change of magnet spacing has little effect on the output voltage of the outer beam. Therefore, PVEH could obtain a high output voltage and an appropriate magnetic spacing range. The second open-circuit output voltage peak in Fig. 4(a) is significantly weakened, and the first open-circuit output voltage peak in Fig. 4(b) is enhanced, compared to the PVEH in different magnet spacing on the output voltage and working bandwidth, $s = 22$ mm is selected due to the obvious gains act in output performance as shown in Fig. 4(d).

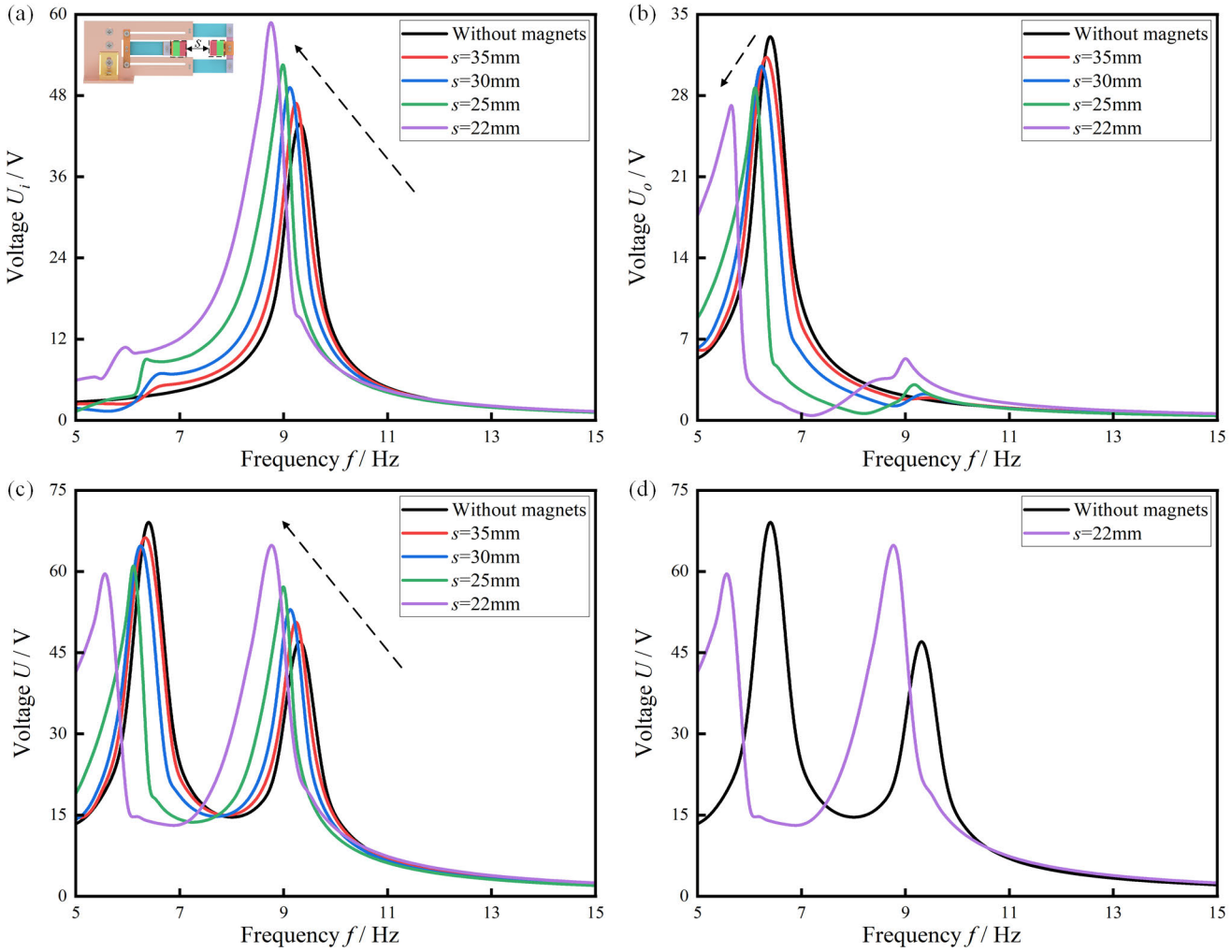

FIGURE 4. The simulation results of changing the magnet spacing: (a)The output voltage of the inner beam;(b) The output voltage of outer beams;(c) The total output voltage of the inner and outer beams; (d) The comparison between the proposed PVEH under the magnetic spacing is 22 mm and the PVEH without magnets.

IV. EXPERIMENTS AND DISCUSSION

The experimental setup is shown in Fig. 5(a) and mainly consists of a power amplifier (L800A), a vibrator (LT-50), a vibration control system (VT-9008), and a PC. The work-flow diagram of the experimental system is shown in Fig. 5(b). First, the control software in the PC generates a sweep signal to control the power amplifier, which acts on the shaker to produce a vibration source. Then, the accelerometer will be used to monitor the acceleration of the shaker and send the acceleration signal back to the vibration control system. At the same time, the output voltage signal generated by the prototype is measured by the vibration control system. Finally, the experimental data of the prototype in the vibration control system is transmitted to the PC for further processing and storage. The prototype production process in Fig. 5(c) is as follows: first, this experiment uses CAD to establish the overall structure model of the prototype, uses the engraving machine to process the acrylic plate, and uses 3D printing to print the connectors, and finally assembles each part (i.e. the tip masses, the piezoelectric sheets, and the magnets). The prototype Table 1 shows the Structural parameters of the PVEH. The material of the piezoelectric beam is shown in

TABLE 1. Structural parameters of the PVEH.

Parameter	Symbol	Value
Inner beam length	L_i	80 mm
Inner beam width	W_i	10 mm
Inner beam thickness	T_i	0.55 mm
Outer beam length	L_o	80 mm
Outer beam width	W_o	10 mm
Outer beam thickness	T_o	0.55 mm
Connection block mass	M_c	1.40 g
Magnetic spacing	s	15 mm-50 mm
Inner beam tip mass	M_i	1.80 g-4.20 g
Outer beam tip mass	M_o	1.80 g-4.20 g

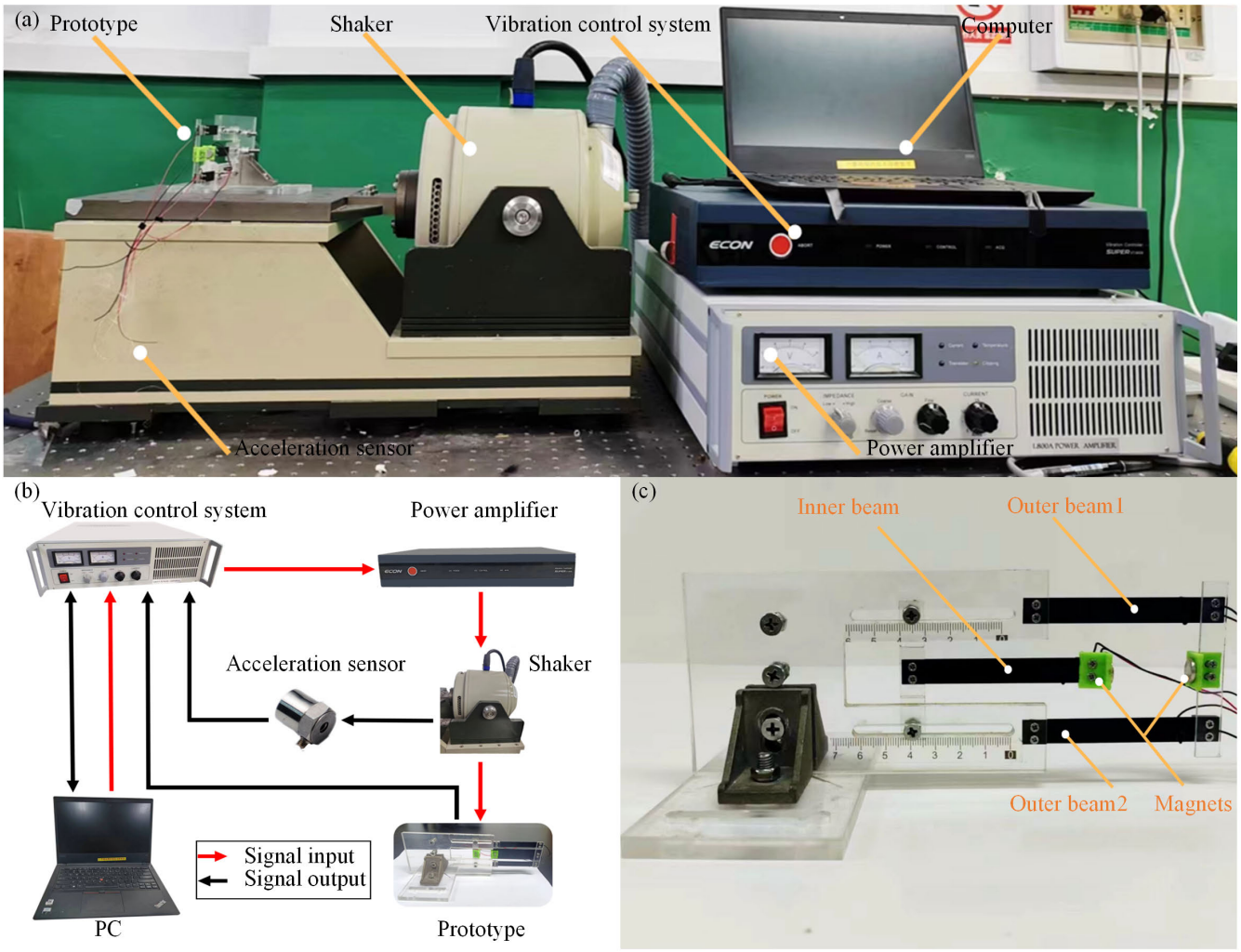

FIGURE 5. (a) Experimental setup;(b) Flow diagram with experimental devices; (c) The proposed prototype of a parallel PVEH based on multi-frequency technique and magnetic nonlinear technique.

Table 2. Besides, the combination of multimodal and nonlinear techniques generates complex output voltage waves, which creates challenges to subsequent energy circuit management. However, this article focuses on the synergy of these two techniques in improving the output performance of the PVEH. Although it is very interesting to explore the circuits that make these two techniques synergistic for energy management work, this article focuses on the coupling coordination of the two techniques.

Fig. 6(a1)-(b3) shows the frequency sweep experimental results of the open-circuit output voltage peak-to-peak value of the inner beam, the outer beam, and the sum of them under different tip masses of the inner and outer beams. When the tip mass of the inner beam (M_i) increases from 2.5 g to 6.7 g in Fig. 6(a1), the second open-circuit output voltage peak made by the resonance of the inner beam moves to the left (8.95 Hz-12.01 Hz) and turns to higher than the original state (31.15 V- 49.05 V). With the increase of the tip mass of the inner beam, not only does the natural frequency of the inner beam but also the output voltage is increased by the growth of the kinetic energy of the system under the condition that the acceleration of the vibration source remains unchanged. Fig. 6(a2) shows that the resonance of the inner beam strengthens the vibration of the outer beam under the action of magnetic coupling, which creates the second voltage peak. Therefore, with the increase of M_i, the second voltage peak of the outer beam also changes like the second peak of the inner beam under this magnetic coupling relationship, which results in the corresponding natural frequency decreasing and the peak voltage increasing. Besides, the first voltage peak produced by the resonance of the outer beam has been restrained, and its natural frequency has little effect. The increase of M_i plays a gain effect on the first voltage peak (31.15 V-49.05 V) in Fig. 6(a1), which is produced by the vibration of the inner beam driven by the resonance of the outer beam. In the sweep frequency range, when $M_i = 6.7$ g, the open-circuit output voltage of the inner beam reaches a maximum of 49.05 V, while the maximum open-circuit output

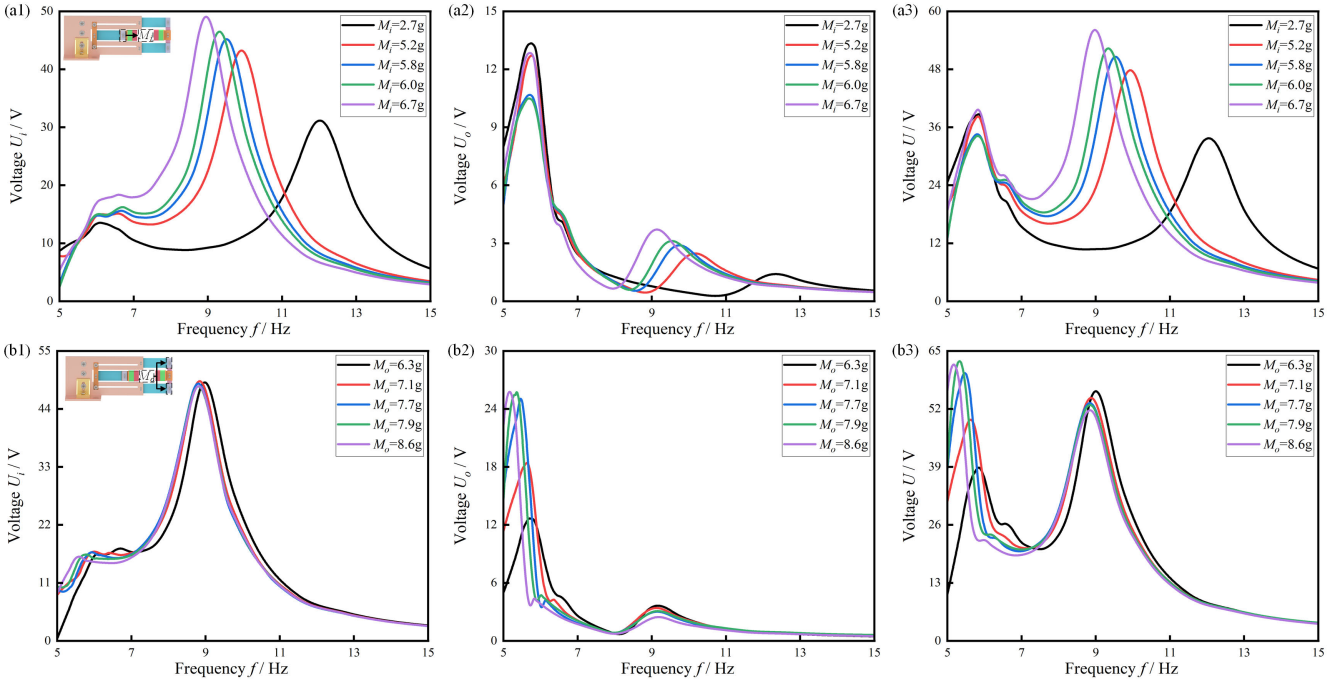

FIGURE 6. The open-circuit output voltage under changing the tip mass of beams: (a1) The output voltage of the inner beam under changing the tip mass of the inner beam; (a2) The output voltage of the outer beam under changing the tip mass of the inner beam; (a3) The total output voltage of the inner beam and outer beams under changing the tip mass of the inner beam; (b1) The output voltage of the inner beam under changing the tip mass of the outer beam; (b2) The output voltage of the outer beam under changing the tip mass of the outer beam; (b3) The total output voltage of the inner beam and outer beams under changing the tip mass of the outer beam.

voltage of the outer beam is at 12.84 V. Fig. 6(a3) presents the change of the overall voltage of the harvester in the range of frequency sweep, which is consistent with the simulation results from Fig. 3(a3) in the third section of this paper. From the point of view of improving the overall output performance of the system, $M_{\mathrm{i}} = 6.7$ g is the optimized mass parameter of the inner beam configuration so that the maximum voltage of the first peak and the second peak can reach 39.65 V and 56.12 V, respectively. Therefore, $M_{\mathrm{i}} = 6.7$ g has been a quality condition in the experiment of exploring the effect of M_{o} on the output performance of PVEH. Fig. 6(b1)-(b3) explores the influence of the tip mass of the outer beam (M_{o}) on the output voltage of the proposed PVEH. When the tip mass of the outer beam increases from 3.2 g to 5.2 g, the first open-circuit output voltage peak of the outer beams in Fig. 6(b2) caused by the resonance of the outer beam moves from 5.16 Hz to 5.75 Hz and increases from 12.66 V to25.76 V. The reason for this change is similar to the rule of increasing M_{i}.

On the one hand, the natural frequency of the outer beam turns smaller; on the other hand, the growth of the kinetic energy of the system under the unchanged acceleration of the vibration source enhances the output voltage by adding the tip mass of the outer beam. Fig. 6(b1) expresses that the resonance of the outer beam strengthens the vibration of the inner beam under the action of magnetic coupling, which produces the first voltage peak of the inner beam. The voltage (17.52 V-15.98 V) and its natural frequency (5.59 Hz-6.69 Hz) decreased by adding the tip mass of the outer beam. Moreover, the second voltage peak in Fig. 6(b2) created by the vibration of the outer beam, which is driven by the resonance of the outer beam under the magnetic coupling, decreases from 3.64 V to 2.47 V, and its natural frequency changes little. It can be found that the increase of M_{o} will play an inhibitory role in this second peak. In the sweep frequency range, the maximum open-circuit voltage of the inner beam is 48.32 V when M_{o} is 5.2 g, and the maximum open-circuit output voltage of the outer beam is 25.76 V. Therefore, the same conclusion can be gained as in the third section simulation. When the tip mass of the cantilever beam increases, the voltage peak of this beam at its resonant frequency increases. Because the tip mass of the inner beam accounts for a large proportion of the total mass, the inner beam plays an important role in the open-circuit output voltage, and the increase of M_{i} initially has an inhibition effect on the outer beam. With the further increase of the tip mass of the inner beams,

TABLE 2. Material parameters of the PVEH.

Properties	Inner beam	Outer beam
Thickness of the piezoelectric layer	0.2 mm*2	0.2 mm*2
Thickness of substrate	0.15 mm	0.15 mm
Material of substrate	Cu	Cu
Material of the piezoelectric layer	PZT	PZT
The material of the magnet	NdFeB magnet	NdFeB magnet

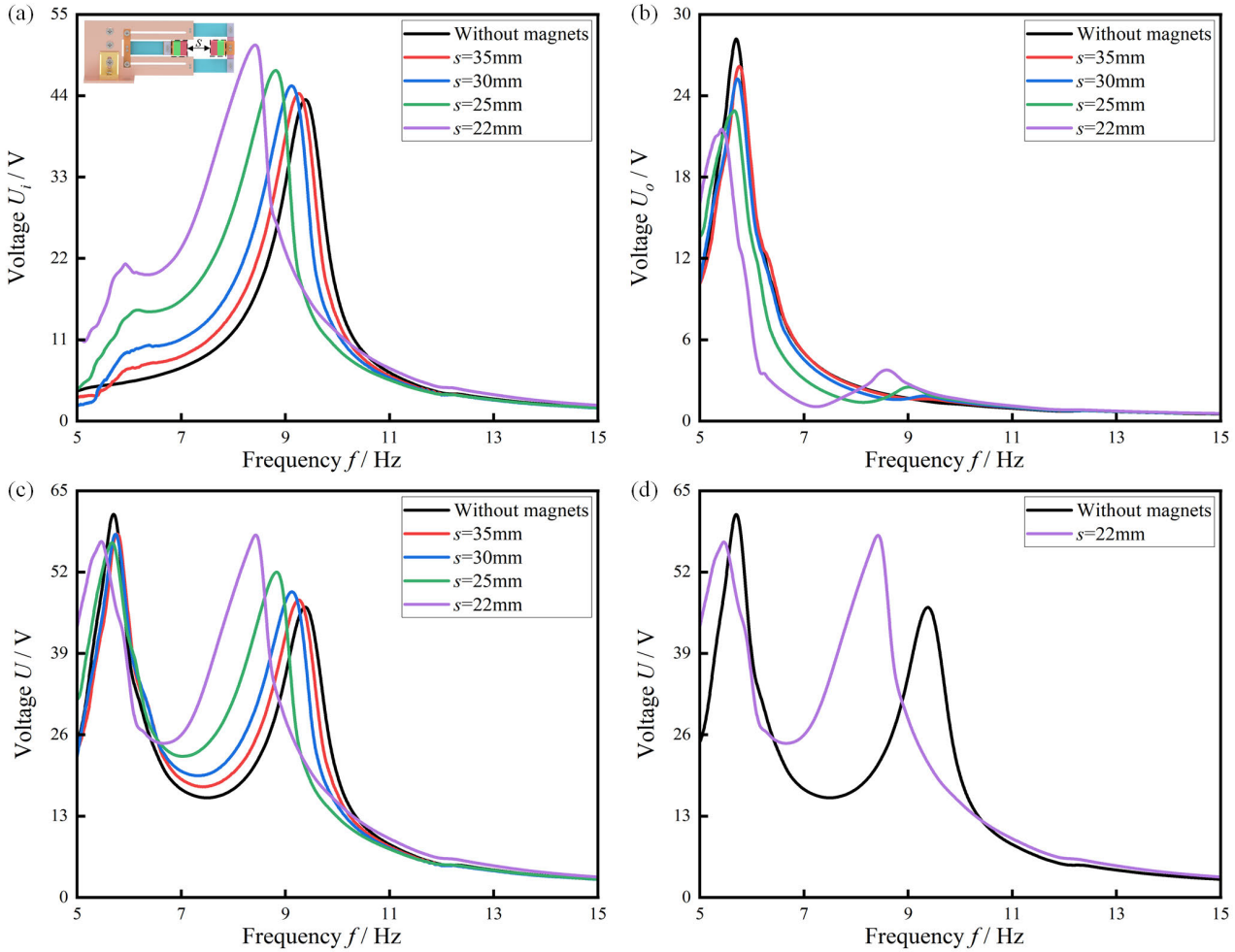

FIGURE 7. The open-circuit output voltage under changing the magnetic spacing: (a)The output voltage of the inner beam; (b) The output voltage of outer beams;(c) The total output voltage of the inner and outer beams; (d) The comparison between the proposed PVEH under the magnetic spacing is 22 mm and the PVEH without magnets.

it augments the output voltage of the outer beam. At the same time, the growth of the M_o has little effect on the output inner beam. It concludes from Fig. 6(b3) that the open circuit output voltage of the first peak is 62.71 V when $M_o = 5.0$ g and the open circuit output voltage of the second peak is 52.87 V. The two peaks are slightly higher than the voltage at $M_o = 5.2$ g. $M_o = 5.0$ g was selected as a quality condition in the experiment of exploring the effect of s on the output performance of PVEH to obtain high output performance and the portability of the system.

Fig. 7 shows the influence of the spacing between the magnets on the peak-to-peak value of the open-circuit output voltage of the inner beam, the outer beam, and the sum of them. In the frequency sweep range, as shown in Fig. 7(a) and 7(b), there is only one peak in the voltage curve of the inner and outer beams without magnets, but there are two peaks under magnetic force. As the spacing between the magnets gradually decreases from 35 mm to 22 mm, the first voltage peak of the inner beam increases from 6.89 V to 21.26 V. In contrast, the second one increases from 21.91 V to 50.85 V, as shown in Fig. 7(a). However, the first voltage peak of the outer beam slowly decreases from 28.19 V to 21.54 V. In contrast, the second one increases from 1.61 V to 3.77 V in Fig. 7(b). The above results indicate that the magnetic repulsive force has a positive gain impact on the voltage and bandwidth of the inner beam but has an inhibiting effect on the outer beams when the magnetic spacing is within the gain range of 22 mm to 35 mm. Fig. 7(c) shows the total voltage change of the harvester with and without magnets, which indicates that the output performance of the second peak caused by the inner beam is significantly enhanced. However, the magnetic force has relatively little effect on the output performance of the first peak determined by the outer beams. The above consequences are consistent with the results from the simulation part. Because the influence of magnet nonlinear coupling on the inner beam is much stronger than on the outer beams. It causes the maximum value on the second peak of the harvester to reach 57.92 V, and the first voltage peak to reach 56.88 V when $s = 22$ mm. Fig. 7(d) shows the output voltage comparison of the harvester under non-magnetic and magnetic conditions ($s = 22$ mm). Compared with the non-magnetic condition, the overall output

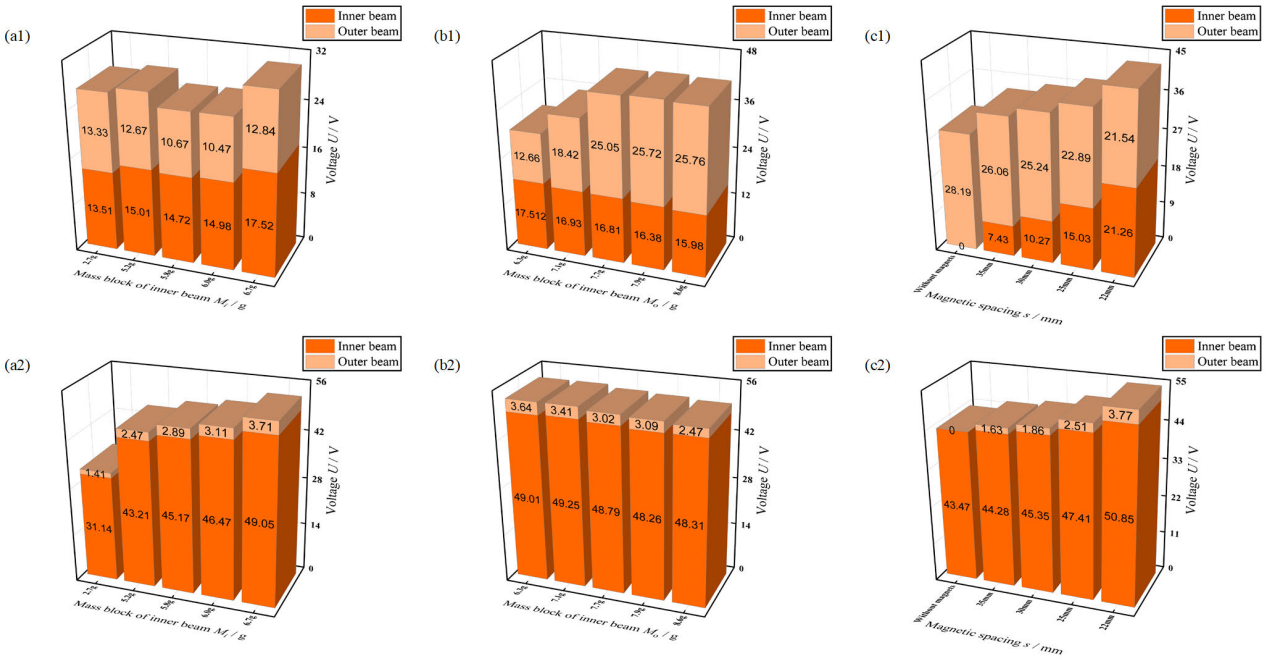

FIGURE 8. The output voltage under different conditions: (a) Changing the tip mass of the inner beam; (b) Changing the tip mass of the outer beam; (c) Changing the magnet spacing.

performance of the harvester has been significantly improved when $s = 22$ mm, which is in good agreement with the simulation results in Fig. 4(d). In detail, the operating bandwidth increases from 1.06 Hz to 1.11 Hz at the first-order operating frequency, and from 1.35 Hz to 1.76 Hz at the second one. Although the voltage decreases slightly near the peak position of the first-order operating frequency, it is improved at the second-order operating frequency. The voltage near the peak position of the second-order operating frequency increases by 30.37 % compared to that of the harvester without magnets. In addition, it should be noted that when the magnet spacing is further reduced to 15 mm or less, the effective vibration of the harvester in experiments is significantly suppressed, resulting in a sharp decrease in the output voltage. Because the magnetic force is too large, the harvester falls into a potential well and hardly achieves efficient power conversion. Therefore, the optimized magnet spacing parameter is selected as 22 mm for obtaining the high-level output performance of the system.

To further explore the influence of the tip mass of beams and magnet spacing on the output performance of the PVEH, the open-circuit voltage peak values of the inner beam and single outer beam under different conditions of tip mass and magnet spacing are shown in Fig. 8. Fig. 8(a1) expresses the variation of the first peak value of voltage curve with the increase of the tip mass of the inner beam. Results show that the output voltage of the outer beam tends to decrease first at the range from $M_i = 5.2$ g to $M_i = 6.0$ g and then increase, while the one of the inner beam is stable. In Fig. 8(a2), the second voltage peak values of the inner beam and the outer beams increase sharply at first and then tend to be flat with the increasing tip mass of the inner beam from 2.7 g to 6.7 g. Besides, the second peak value of the voltage of the inner beam is much larger than that of the outer beams. So, the increase of the tip mass of the inner beam significantly improves its output voltage at the second-order operating frequency, which corresponds to the natural frequency of the inner beam.

Fig. 8(b1) shows the voltage curve with the increase of the tip mass of the outer beam. The output voltage of the outer beam at the first-order frequency increases significantly in the range from $M_o = 6.3$ g to $M_o = 7.7$ g and then tends to be stable, while the voltage of the inner beam does not change much. The increase of the tip mass blocks will strengthen the vibration of the beams, improving the output voltages. Besides, Fig. 8(b2) indicates that the output voltage of the inner and outer beams at the second-order operating frequency is almost unchanged.

Fig. 8(c1) and Fig. 8(c2) show the output voltage of the beams at the first-order and second-order operating frequencies, respectively, when the magnet spacing changes. With the decrease of the magnet spacing, the output voltage of the inner beam at the first-order operating frequency increases, while the output voltage of the outer beam slightly decreases. At the first-order operating frequency, the outer beam will be driven to vibrate due to the resonance of the inner beam. Conversely, the inner beam is driven to vibrate at the second-order frequency because of the resonance of the outer beam. This phenomenon will obviously increase the output voltage of the PVEH when the magnetic spacing decreases. The reason is that the magnetic force will bring a gain effect to the vibration or deformation of the beam in most cases when the magnetic force increases. The magnetic spacing becomes close and the

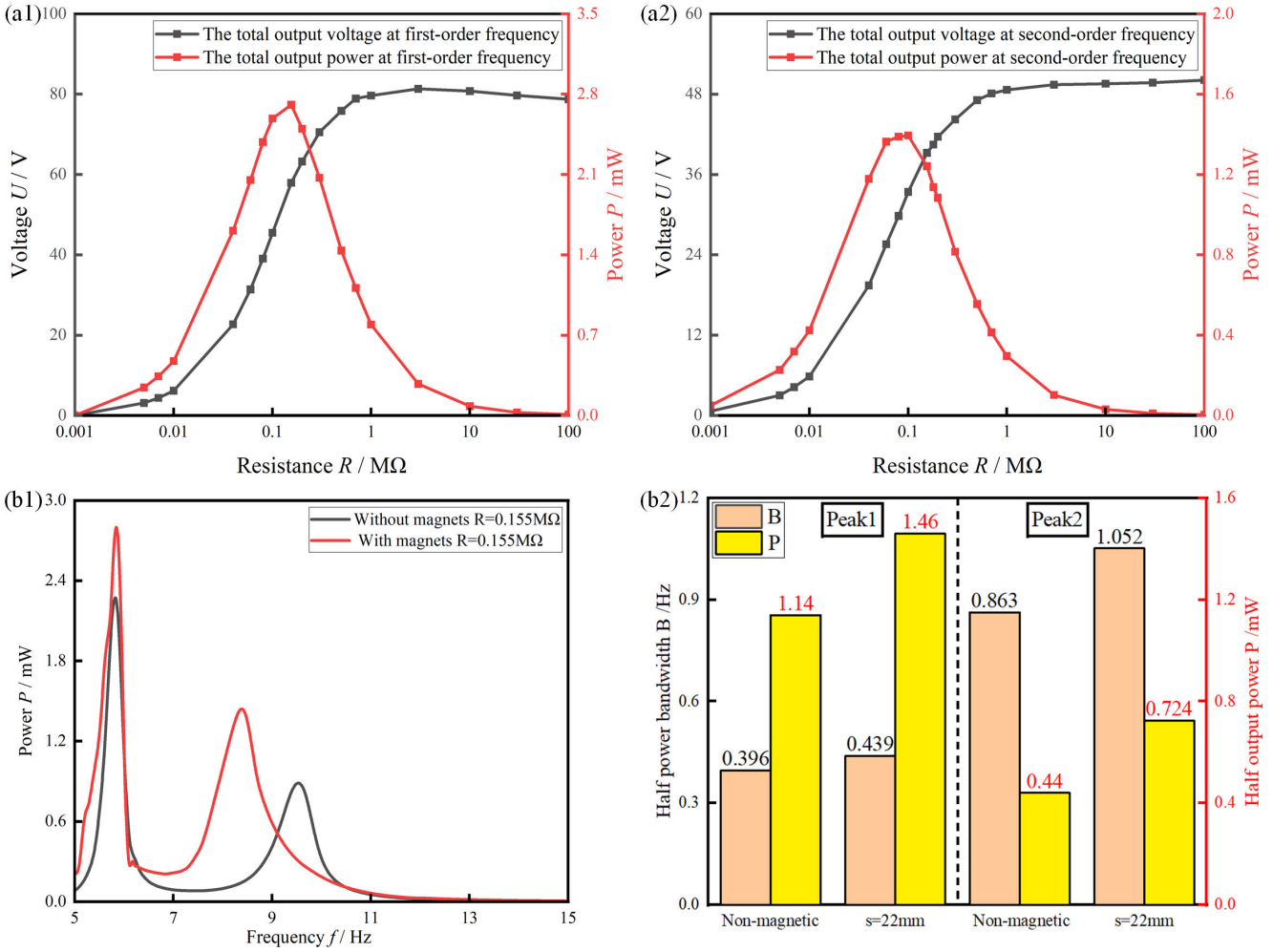

FIGURE 9. Impedance matching results: The load voltage and the output power response at (a1) 6.2 Hz and (a2) 8.6 Hz; (b1) Comparison of output power with or without magnetic mode (R = 0.155 MΩ); (b2) Half power bandwidth.

magnetic force will increase, which expands this gain effect, therefore the output performance of the PVEH increases. Combined with (5), it can be found that the magnet spacing decreases and the magnetic force will increase.

Fig. 9. shows the output voltage and power of the proposed PVEH connected with different load resistances under optimized structural parameters (s = 22 mm, M_i = 6.7 g, M_o = 5.0 g). With the increase of load resistance, the sum of the output voltages firstly increases and then approaches a stable value, which is 79.68 V at the first-order operating frequency in Fig. 9(a1), and 50.11 V at the second-order operating frequency in Fig. 9(a2). When the excitation frequency is 6.2 Hz, as given in Fig. 9(a1), the output power rises rapidly and declines. The maximum sum of the output power of the three piezoelectric beams reaches 2.80 mW under the optimal load resistance of 0.155 MΩ. In addition, when the excitation frequency is 8.6 Hz, and the optimal load resistance is 0.155 MΩ, the sum of the output power of the three piezoelectric beams is 1.44 mW. From the above results, the output power at the first-order operating frequency is much greater than at the second-order operating frequency. The reason is that the magnet coupling has an obvious promotion of enhancing the output voltage of the inner beam. Lastly, the load resistance of the inner and outer beams is selected as 0.155 MΩ. As shown in Fig. 9(b1), the output power with the magnetic structure at the first-order operating frequency is rapidly improved from 2.27 mW to 2.80 mW compared to the non-magnetic structure. When the excitation frequency is equal to the second-order operating frequency, the output power in the magnetic structure is improved from 0.88 mW to 1.42 mW compared to the non- magnetic structure. From Fig. 9(b2), comparing the proposed PVEH with the non-magnetic mode, the half-power bandwidth of the PVEH increases from 0.396 Hz to 0.439 Hz at the first-order operating frequency, and from 0.863 Hz to 1.052 Hz at the second-order operating frequency. Thus, the bandwidth increases by 9.70% and 21.90% at the first-order and second-order operating frequencies, respectively. At the same time,

TABLE 3. Output performance comparison of similar structures.

Ref.	V-Volume of all beams (mm^3)	a - Acceleration(g m/s^2)	U_{max}-Maximum voltage (V)	P_{max}-Maximum power (mW)	Pmax/V ($\mu W/mm^3$)	Pmax/a (mW/g)	Pmax/V/a ($\mu W/mm^3/g$)
[45]	3064	0.3	/	1.70	$5.5*10^{-1}$	5.67	1.83
[46]	155	0.3	8	/	/	/	/
[47]	3609	/	22	1.90	$5.3*10^{-1}$	/	/
[48]	1520	0.2	60	$5*10^{-2}$	$3.0*10^{-2}$	$2.5*10^{-1}$	$1.5*10^{-1}$
[49]	/	0.2	/	1.00	/	5.00	/
[50]	564	0.1	$2*10^{-3}$	$1.5*10^{-4}$	$2.7*10^{-4}$	$1.5*10^{-3}$	$2.7*10^{-3}$
[51]	1520	0.1	28.4	/	/	/	/
This work	1320	0.2	80	2.80	2.12	14.00	1.06*10

the half-output power of the proposed harvester increases from 1.14 mW to 1.46 mW at the first-order operating frequency and increases from 0.44 mW to 0.724 mW at the second-order operating frequency. This means that the output power increases by 28.07% and 64.54% at the first-order and second-order operating frequencies, respectively. Hence, the proposed parallel piezoelectric vibration energy harvester has higher output power and a better broadband effect than the PVEH without magnets.

In addition, Table 3 shows the results that compared with other similar structures, the volume part in the table is calculated as the volume sum of all power generation beams, and the maximum output voltage or power is the sum of maximum output voltage or power of all the beams. The maximum output power per unit volume and the maximum output power per unit acceleration are calculated, and the data manifests that the parallel PVEH proposed in this paper also has great advantages on average output power. Comparing the maximum output power per unit volume and unit acceleration, the results of the proposed harvester are better than the other articles listed. The maximum output power of this paper is 64.70% higher than that of the reference [45]. All the results discussed above indicate the designed parallel PVEH in this work obtains higher output power and bandwidth compared to the counterparts consisting of similar multi-beams parallel structures with magnets. The essential reason for the significant improvement of the output performance of the device stems from the cooperative utilization of the advantages of the multi-frequency technique and the magnetic nonlinear technique and the systematic optimization of the structure parameters.

V. CONCLUSION

A piezoelectric vibration energy harvester combining multi-frequency and magnetic nonlinear techniques is proposed in this paper to reveal the coupling mechanism of these two techniques. The three key parameters of the harvester (i.e. the tip mass of the inner beam, the tip mass of the outer beam, and magnet spacing) are first obtained through the theoretical model analysis. The results of the simulation and experiment indicate that an increase in the tip mass of the beams improves the output performance of the corresponding beam. Besides, the decrease of the magnetic spacing results in the increase of the magnetic force, and the output power and half-power bandwidth of the proposed energy harvester can be enhanced when the magnet spacing is within the gain range. The maximum output power of the proposed PVEH reaches 2.80 mW at the first-order operating frequency and 1.42 mW at the second-order operating frequency by optimizing the parameters of the system, which enhances by 23.35% and 38.10% compared to the non-magnetic structure. The maximum output power and half-power bandwidth of this harvester have great advantages compared with other same-type harvesters with similar structures. This paper provides meaningful guidance for the design and practical application of this vibration energy harvester.

ACKNOWLEDGMENT

(Yili Hu and Yaru Ding contributed equally to this work.)

REFERENCES

[1] D. Hao, L. Kong, Z. Zhang, W. Kong, A. M. Tairab, X. Luo, A. Ahmed, and Y. Yang, "An electromagnetic energy harvester with a half-wave rectification mechanism for military personnel," *Sustain. Energy Technol. Assessments*, vol. 57, Jun. 2023, Art. no. 103184.
[2] L. Chen, Y. Ma, C. Hou, X. Su, and H. Li, "Modeling and analysis of dual modules cantilever-based electrostatic energy harvester with stoppers," *Appl. Math. Model.*, vol. 116, pp. 350–371, Apr. 2023.
[3] H. Abumarar and A. Ibrahim, "A nonlinear impact-driven triboelectric vibration energy harvester for frequency up-conversion," *Micromachines*, vol. 14, no. 5, p. 1082, May 2023.
[4] C. S. Clemente, I. Iannone, V. P. Loschiavo, and D. Davino, "Design and optimization of a boost interface for magnetostrictive energy harvesting," *Appl. Sci.*, vol. 13, no. 3, p. 1606, Jan. 2023.
[5] N. Batra, R. S. Deol, M. Singh, and B. Mitra, "Mechanically coupled cantilever beam structure for piezoelectric energy harvesting," *J. Micromech. Microeng.*, vol. 33, no. 3, Mar. 2023, Art. no. 034001.

[6] W. Zhou, D. Du, Q. Cui, Z. Yang, C. Lu, Y. Wang, and Q. He, "Piezoelectric vibration energy harvester: Operating mode, excitation type and dynamics," *Adv. Mech. Eng.*, vol. 14, no. 10, Oct. 2022, Art. no. 168781322211311.

[7] S. Sharma, R. Kiran, P. Azad, and R. Vaish, "A review of piezoelectric energy harvesting tiles: Available designs and future perspective," *Energy Convers. Manage.*, vol. 254, Feb.15, 2022, Art. no. 115272.

[8] X. Liu, L. He, R. Liu, D. Hu, L. Zhang, and G. Cheng, "Piezoelectric energy harvesting systems using mechanical tuning techniques," *Rev. Sci. Instrum.*, vol. 94, no. 3, Mar. 2023, Art. no. 031501.

[9] J. Jiang, S. Liu, L. Feng, and D. Zhao, "A review of piezoelectric vibration energy harvesting with magnetic coupling based on different structural characteristics," *Micromachines*, vol. 12, no. 4, p. 436, Apr. 2021.

[10] M. S. Salem, S. Ahmed, A. Shaker, M. T. Alshammari, K. A. Al-Dhlan, A. Alanazi, A. Saeed, and M. Abouelatta, "Bandwidth broadening of piezoelectric energy harvesters using arrays of a proposed piezoelectric cantilever structure," *Micromachines*, vol. 12, no. 8, p. 973, Aug. 2021.

[11] D.-X. Cao, W. Xia, X.-Y. Guo, and S.-K. Lai, "Modeling and experiment of vibro-impact vibration energy harvester based on a partial interlayer-separated piezoelectric beam," *J. Intell. Mater. Syst. Struct.*, vol. 32, no. 8, pp. 817–831, May 2021.

[12] V. J. Caetano and M. A. Savi, "Multimodal pizza-shaped piezoelectric vibration-based energy harvesters," *J. Intell. Mater. Syst. Struct.*, vol. 32, no. 20, pp. 2505–2528, Dec. 2021.

[13] V. J. Caetano and M. A. Savi, "Star-shaped piezoelectric mechanical energy harvesters for multidirectional sources," *Int. J. Mech. Sci.*, vol. 215, Feb. 2022, Art. no. 106962.

[14] K. Hu and M. Wang, "Broadband piezoelectric energy harvester based on coupling resonance frequency tuning," *Micromachines*, vol. 14, no. 1, p. 105, Dec. 2022.

[15] Y. Cheng, N. Wu, and Q. Wang, "An efficient piezoelectric energy harvester with frequency self-tuning," *J. Sound Vibrat.*, vol. 396, pp. 69–82, May 2017.

[16] Y.-H. Shin, J. Choi, S. J. Kim, S. Kim, D. Maurya, T.-H. Sung, S. Priya, C.-Y. Kang, and H.-C. Song, "Automatic resonance tuning mechanism for ultra-wide bandwidth mechanical energy harvesting," *Nano Energy*, vol. 77, Nov. 2020, Art. no. 104986.

[17] S. Pyo, D.-S. Kwon, H.-J. Ko, Y. Eun, and J. Kim, "Frequency up-conversion hybrid energy harvester combining piezoelectric and electromagnetic transduction mechanisms," *Int. J. Precis. Eng. Manuf.-Green Technol.*, vol. 9, no. 1, pp. 241–251, Jan. 2022.

[18] J. Liu, Y. Lu, Z. Wang, S. Li, and Y. Wu, "Three frequency up-converting piezoelectric energy harvesters caused by internal resonance mechanism: A narrative review," *Micromachines*, vol. 13, no. 2, p. 210, Jan. 2022.

[19] M. Rosso, A. Corigliano, and R. Ardito, "Numerical and experimental evaluation of the magnetic interaction for frequency up-conversion in piezoelectric vibration energy harvesters," *Meccanica*, vol. 57, no. 5, pp. 1139–1154, May 2022.

[20] G. Shan and M. Zhu, "A piezo stack energy harvester with frequency up-conversion for rail track vibration," *Mech. Syst. Signal Process.*, vol. 178, Oct. 2022, Art. no. 109268.

[21] O. Pertin, K. Guha, O. Jakšić, Z. Jakšić, and J. Iannacci, "Investigation of nonlinear piezoelectric energy harvester for low-frequency and wideband applications," *Micromachines*, vol. 13, no. 9, p. 1399, Aug. 2022.

[22] M. Bonnin, F. L. Traversa, and F. Bonani, "An impedance matching solution to increase the harvested power and efficiency of nonlinear piezoelectric energy harvesters," *Energies*, vol. 15, no. 8, p. 2764, Apr. 2022.

[23] K. Chen, S. Fang, Q. Gao, D. Zou, J. Cao, and W.-H. Liao, "An enhanced nonlinear piezoelectric energy harvester with multiple rotating square unit cells," *Mech. Syst. Signal Process.*, vol. 173, Jul. 2022, Art. no. 109065.

[24] S. Sun, Y. Leng, S. Hur, F. Sun, X. Chen, H.-C. Song, and C.-Y. Kang, "Force and stability mechanism analysis of two types of nonlinear monostable and multi-stable piezoelectric energy harvesters using cantilever structure and magnetic interaction," *Smart Mater. Struct.*, vol. 32, no. 3, Mar. 2023, Art. no. 035003.

[25] H.-K. Shim, S. Sun, H.-S. Kim, D.-G. Lee, Y.-J. Lee, J.-S. Jang, K.-H. Cho, J. M. Baik, C.-Y. Kang, Y. Leng, S. Hur, and H.-C. Song, "On a nonlinear broadband piezoelectric energy harvester with a coupled beam array," *Appl. Energy*, vol. 328, Dec.15, 2022, Art. no. 120129.

[26] M. Ferrari, V. Ferrari, M. Guizzetti, D. Marioli, and A. Taroni, "Piezoelectric multifrequency energy converter for power harvesting in autonomous microsystems," *Sens. Actuators A, Phys.*, vol. 142, no. 1, pp. 329–335, Mar. 2008.

[27] T. Kim, Y. Ko, C. Yoo, B. Choi, S. Han, and N. Kim, "Design optimisation of wide-band piezoelectric energy harvesters for self-powered devices," *Energy Convers. Manage.*, vol. 225, Dec. 2020, Art. no. 113443.

[28] P. Wang, X. Liu, H. Zhao, W. Zhang, X. Zhang, Y. Zhong, and Y. Guo, "A two-dimensional energy harvester with radially distributed piezoelectric array for vibration with arbitrary in-plane directions," *J. Intell. Mater. Syst. Struct.*, vol. 30, no. 7, pp. 1094–1104, Apr. 2019.

[29] R. M. Toyabur, M. Salauddin, and J. Y. Park, "Design and experiment of piezoelectric multimodal energy harvester for low frequency vibration," *Ceram. Int.*, vol. 43, pp. S675–S681, Aug. 2017.

[30] V. Raja, M. Umapathy, G. Uma, and R. Usharani, "Design, modeling, and experimental verification of reversed exponentially tapered multimodal piezoelectric energy harvester from harmonic vibrations for autonomous sensor systems," *Int. J. Mech. Mater. Design*, vol. 19, no. 4, pp. 763–792, Dec. 2023.

[31] X. Huang, C. Zhang, and K. Dai, "A multi-mode broadband vibration energy harvester composed of symmetrically distributed U-shaped cantilever beams," *Micromachines*, vol. 12, no. 2, p. 203, Feb. 2021.

[32] S. Zhou, J. D. Hobeck, J. Cao, and D. J. Inman, "Analytical and experimental investigation of flexible longitudinal zigzag structures for enhanced multi-directional energy harvesting," *Smart Mater. Struct.*, vol. 26, no. 3, Mar. 2017, Art. no. 035008.

[33] C. Lan, Y. Liao, G. Hu, and L. Tang, "Equivalent impedance and power analysis of monostable piezoelectric energy harvesters," *J. Intell. Mater. Syst. Struct.*, vol. 31, no. 14, pp. 1697–1715, Aug. 2020.

[34] H. Wang and L. Tang, "Modeling and experiment of bistable two-degree-of-freedom energy harvester with magnetic coupling," *Mech. Syst. Signal Process.*, vol. 86, pp. 29–39, Mar. 2017.

[35] Q. Zhu, G. Wang, Y. Zheng, Z. Liu, S. Zhou, and B. Zhang, "Coupling nonlinearities and dynamics between the hybrid tri-stable piezoelectric energy harvester and nonlinear interfaced circuit," *Appl. Energy*, vol. 323, Oct. 2022, Art. no. 119636.

[36] D. Upadrashta and Y. Yang, "Nonlinear piezomagnetoelastic harvester array for broadband energy harvesting," *J. Appl. Phys.*, vol. 120, no. 5, Aug. 2016, Art. no. 054504.

[37] S. K. Lim and H. H. Yoo, "Modeling and performance analysis of a novel M-shaped piezoelectric energy harvester employing magnets," *J. Mech. Sci. Technol.*, vol. 34, no. 9, pp. 3553–3563, Sep. 2020.

[38] K.-Q. Fan, F.-B. Chao, J.-G. Zhang, W.-D. Wang, and X.-H. Che, "Design and experimental verification of a bi-directional nonlinear piezoelectric energy harvester," *Energy Convers. Manage.*, vol. 86, pp. 561–567, Oct. 2014.

[39] Q. He and T. Jiang, "Complementary multi-mode low-frequency vibration energy harvesting with chiral piezoelectric structure," *Appl. Phys. Lett.*, vol. 110, no. 21, May 2017, Art. no. 213901.

[40] A. Erturk and D. J. Inman, "On mechanical modeling of cantilevered piezoelectric vibration energy harvesters," *J. Intell. Mater. Syst. Struct.*, vol. 19, no. 11, pp. 1311–1325, Nov. 2008.

[41] X. Xiong and S. O. Oyadiji, "Modal electromechanical optimization of cantilevered piezoelectric vibration energy harvesters by geometric variation," *J. Intell. Mater. Syst. Struct.*, vol. 25, no. 10, pp. 1177–1195, Jul. 2014.

[42] D. Tan, Y. G. Leng, and Y. J. Gao, "Magnetic force of piezoelectric cantilever energy harvesters with external magnetic field," *Eur. Phys. J. Special Topics*, vol. 224, nos. 14–15, pp. 2839–2853, Nov. 2015.

[43] K. W. Yung, P. B. Landecker, and D. D. Villani, "An analytic solution for the force between two magnetic dipoles," *Magn. Electr. Separat.*, vol. 9, no. 1, pp. 39–52, 1998.

[44] S. C. Stanton, C. C. McGehee, and B. P. Mann, "Nonlinear dynamics for broadband energy harvesting: Investigation of a bistable piezoelectric inertial generator," *Phys. D, Nonlinear Phenomena*, vol. 239, no. 10, pp. 640–653, May 2010.

[45] W.-J. Su, J. Zu, and Y. Zhu, "Design and development of a broadband magnet-induced dual-cantilever piezoelectric energy harvester," *J. Intell. Mater. Syst. Struct.*, vol. 25, no. 4, pp. 430–442, Mar. 2014.

[46] K.-Q. Fan, C.-H. Xu, W.-D. Wang, and Y. Fang, "Broadband energy harvesting via magnetic coupling between two movable magnets," *Chin. Phys. B*, vol. 23, no. 8, Aug. 2014, Art. no. 084501.

[47] L. Zhao, L. Tang, and Y. Yang, "Enhanced piezoelectric galloping energy harvesting using 2 degree-of-freedom cut-out cantilever with magnetic interaction," *Jpn. J. Appl. Phys.*, vol. 53, no. 6, Jun. 2014, Art. no. 060302.

[48] H. Wu, L. Tang, Y. Yang, and C. K. Soh, "Development of a broadband nonlinear two-degree-of-freedom piezoelectric energy harvester," *J. Intell. Mater. Syst. Struct.*, vol. 25, no. 14, pp. 1875–1889, Sep. 2014.
[49] Y. Wu, H. Ji, J. Qiu, and L. Han, "A 2-degree-of-freedom cubic nonlinear piezoelectric harvester intended for practical low-frequency vibration," *Sens. Actuators A, Phys.*, vol. 264, pp. 1–10, Sep. 2017.
[50] M. Atmeh, A. Ibrahim, and A. Ramini, "Static and dynamic analysis of a bistable frequency up-converter piezoelectric energy harvester," *Micromachines*, vol. 14, no. 2, p. 261, Jan. 2023.
[51] M. Krishnasamy, D. Upadrashta, Y. Yang, and T. R. Lenka, "Distributed parameter modelling of cutout 2-DOF cantilevered piezo-magneto-elastic energy harvester," *J. Microelectromech. Syst.*, vol. 27, no. 6, pp. 1160–1170, Dec. 2018.

YILI HU received the B.S. and M.S. degrees from Zhejiang Normal University, in 2012 and 2015, respectively, and the Ph.D. degree in engineering from Shanghai Jiao Tong University, China, in 2020. He has been engaged in the research of piezoelectric actuator and control technology, piezoelectric/triboelectric power generation, and sensing technology for a long time. He is currently an Associate Professor with Zhejiang Normal University.

YARU DING was born in Bengbu, China, in 2001. She is currently pursuing the bachelor's degree with Zhejiang Normal University, Jinhua. Her research interest includes piezoelectric energy harvesting.

NAN WEI received the B.S. degree from the Nanjing University of Information Science and Technology, China, in 2021. She is currently pursuing the M.S. degree with Zhejiang Normal University. Her research interest includes piezoelectric/triboelectric energy harvesting.

XINHUI LI was born in Jiangxi, China, in 1988. He received the B.S. degree in mechanical design, manufacturing and automation and the M.S. degree in physical electronics from Zhejiang Normal University, Jinhua, China, in 2007 and 2011, respectively. He is currently a Lecturer with the Xingzhi College Zhejiang Normal University, Jinhua. His current research interests include piezoelectric actuators and energy harvesters.

JIANPING LI (Member, IEEE) was born in Jiangsu, China, in 1987. He received the B.S. and Ph.D. degrees from the School of Mechanical Science and Engineering, Jilin University, Changchun, China, in 2011 and 2016, respectively. After that, he was a JSPS Researcher with Chiba University, Japan, supported by the Japan Society for the Promotion of Science (JSPS). In 2018, he came back to China and currently with the Institute of Precision Machinery and Smart Structure, College of Engineering, Zhejiang Normal University. His current research interests include piezoelectric actuator-based nano-positioning systems and the application of electrical impedance spectroscopy in biomedical science.

JIJIE MA was born in Tianjin, China, in 1980. He received the Ph.D. degree in mechanical engineering from Jilin University, Changchun, China, in 2010. He is currently an Associate Professor with Zhejiang Normal University, Jinhua, China. His research interests include triboelectric nanogenerators, piezoelectric actuators, and motors.

ZHONGHUA ZHANG received the B.S. degree in mechanical engineering and the M.S. degree in mechanical and electrical engineering from Liaoning Technical University, China, in 2002 and 2005, respectively, and the Ph.D. degree in mechanical and electrical engineering from the Dalian University of Technology, China, in 2009. He is currently an Associate Professor with Zhejiang Normal University, China. He is also with the University of Southampton, U.K., as an Academic Visitor, where he is devoting himself to the research work of piezoelectric energy harvesting. He has published over 30 scientific articles. His main research interests include piezoelectric energy harvesting, piezoelectric pumps, and the integration technology of sensors and actuators.

GUANGMING CHENG was born in 1957. He received the B.S., M.S., and Ph.D. degrees from the Jilin University of Technology, China, in 1982, 1985, and 1996, respectively. He is currently a Professor and a Supervisor for Ph.D. students with Zhejiang Normal University. He has supervised over 15 research projects, including several "863 Program" and "National Natural Science Foundation Program" of China and published more than 70 scientific and technical papers in recent years. His main research interests include theory of piezoelectric actuation technology, micro mechanic-electronic-hydraulic systems, and tribology.

JIANMING WEN was born in Hebei, China, in 1980. He received the B.S. degree in mechanical engineering and automation and the M.S. and Ph.D. degrees in mechanical and electronic engineering from Jilin University, Changchun, China, in 2003, 2006, and 2009, respectively. He is currently a Professor with Zhejiang Normal University, Jinhua, China. His current research interests include piezoelectric drive and control technology.